Published in final edited form as:

Mol Pharm. 2016 December 05; 13(12): 4231–4235. doi:10.1021/acs.molpharmaceut.6b00747.

Self-Targeted Polysaccharide Prodrug Suppresses Orthotopic Hepatoma

Di Li[†,‡], **Weiguo Xu**[†], **Pengqiang Li**[†], **Jianxun Ding**[†,*], **Zhiliang Cheng**[§], **Li Chen**[‡], **Lesan Yan**[§,*], and **Xuesi Chen**[†]

[†]Key Laboratory of Polymer Ecomaterials, Changchun Institute of Applied Chemistry, Chinese Academy of Sciences, Changchun 130022, P. R. China

[‡]Department of Chemistry, Northeast Normal University, Changchun 130024, P. R. China

[§]Department of Bioengineering, University of Pennsylvania, Philadelphia, Pennsylvania 19104-6321, United States

Abstract

Self-targetability is an emerging targeting strategy for polymer nanocarriers with facile preparation and high targeting efficiency. An acid-sensitive dextran–doxorubicin prodrug (Dex-*g*-DOX) has been synthesized and used as a self-targeted drug delivery system for the treatment of orthotopic hepatoma. The polysaccharide prodrug exhibits ultraselective accumulation in cancerous liver tissue, acid-sensitive DOX release within cells, and high antitumor efficacy *in vitro* and *in vivo*. Therefore, Dex-*g*-DOX demonstrates great potential for chemotherapy of orthotopic hepatoma.

Keywords

polysaccharide; prodrug; self-targetability; orthotopic hepatoma; chemotherapy

Polymer–drug conjugates have emerged as highly effective drug delivery platforms that improve therapeutic efficacy and reduce side effects.[1] To date, a wide variety of polymers have been conjugated to a number of preclinical and clinical drugs, including cytotoxics/antineoplastics, antibiotics, immunosuppressants, hormones, nucleic acids, and many others.[2] One of the most widely used polymers for these purposes is the natural polymer dextran (Dex).[3,4] Also, the targeting conjugates bearing antitumor agents can be classified into several groups based on the type of cancer recognition moieties. The targeting moieties usually include monoclonal antibodies, peptides, folate acid, sugars, and so on.[5] However, in general case, targeting polymer prodrugs are prepared going through a series of synthetic

[*]Corresponding Authors: jxding@ciac.ac.cn. Tel/Fax: +86 431 8526 2116. lesanyan@gmail.com. Tel: +1 (215) 573 0290.

Author Contributions

The manuscript was written through contributions of all authors.

Notes

The authors declare no competing financial interest.

Supporting Information

The Supporting Information is available free of charge on the ACS Publications website at DOI: 10.1021/acs.molpharmaceut.6b00747. Experimental details and additional figures (PDF)

steps complicatedly. Moreover, the targeting ability might be affected by various factors *in vivo*, for instance, serum proteins[6] and tumor types.[5] In addition to this, some polymers themselves can also recognize and accumulate in targeting sites specifically. For example, the conjugates modified by Dex can be located in liver in amounts of studies of its kind.[7,8] Based on this, the particular ability of Dex can bring the advantage in the treatment of hepatic diseases. The orthotopic hepatoma, as a primary cancer, is one kind of the deadliest cancers worldwide.[9] Although the surgical resection, ablative therapies, liver transplantation, and other therapeutic methods are implemented widely, hepatoma has a poor prognosis due to rapid progression and frequent hematogenous metastasis.[10]

Herein, a Dex-modified antineoplastic drug doxorubicin (DOX) was developed, forming the polymer–drug conjugate Dex-*g*-DOX through a facile and efficient condensation reaction between Dex and *cis*-aconitic anhydride-modified DOX (CAD). Notably, these two moieties were connected through an acid-cleavable amide bond. As depicted in Scheme 1, the obtained conjugate self-assembled into micellar nanoparticle under physiological conditions. The use of Dex made the conjugate inherently self-targeting, which allowed high accumulation of Dex-*g*-DOX in the liver. Furthermore, because of the acid-responsive amide linker, Dex-*g*-DOX could selectively release DOX within acidic endosomes or lysosomes following endocytosis, granting enhanced delivery of DOX to tumor cells. Altogether, the acid-sensitive Dex-*g*-DOX exhibits great potential for the clinical chemotherapy of hepatoma.

The chemical structure of Dex-*g*-DOX was confirmed by proton nuclear magnetic resonance (^{1}H NMR) and Fourier-transform infrared (FT-IR) spectra. As shown in Figure S1A, Supporting Information, the characteristic peaks at 5.2–4.2 and 3.8–3.4 ppm were assigned to the protons in Dex. The resonances from 7.93–7.65 ppm are typical signals of DOX, indicating the successful attachment of DOX to Dex. In FT-IR spectra (Figure S1B, Supporting Information), the signals at 1640 and 1559 cm^{-1} were assigned to the stretching vibrations of –C=O and –CO–NH– in CAD, respectively, demonstrating its presence in Dex-*g*-DOX. The drug binding content (DBC) of Dex-*g*-DOX was determined to be 12.0 wt % from a ultraviolet–visible (UV–vis) by a standard curve method. In addition, drug binding efficiency (DBE) and drug binding rate (DBR) were calculated to be 78.2 wt % and 3.9%, respectively. All the above information confirmed that the targeting conjugate was synthesized successfully.

The amphiphilic Dex-*g*-DOX could spontaneously self-assemble in an aqueous environment, and micelle was therefore formed by a direct dissolution method. As shown in Figure 1, transmission electron microscopy (TEM) micrograph revealed that the Dex-*g*-DOX micelle has near-spherical morphology. The apparent mean diameter of Dex-*g*-DOX micelle from TEM measurement was detected to be about 90 nm. In comparison, the hydrodynamic diameter (D_h) of Dex-*g*-DOX micelle was 102.0 ± 6.2 nm, as tested by dynamic light scattering (DLS; Figure 1, insert). This size discrepancy indicates minor contraction or swelling of the micelle in the absence (TEM) or presence (DLS) of aqueous solvent, respectively. Furthermore, the critical micelle concentration (CMC) value was determined to be 5.47 μg mL^{-1} by a surface tension technique (Figure S2, Supporting Information), confirming the formation of the micelle. Prior to evaluating whether this prodrug micelle is a

suitable antitumor agent for *in vitro* or *in vivo* studies, the stability of as-prepared micelle was evaluated in phosphate-buffered saline (PBS) at different pH values. As shown in Figure S3, there was no observable change in the size for Dex-*g*-DOX micelle in PBS at pH 7.4 for 120 h, while the obvious swelling and even disassembly were observed at lower pH values (e.g., pH 6.8, 5.0, and 4.0) within the same time frame, suggesting that the micelle is stable at physiological pH and the drug could be released at acidic cancerous environment. Overall, this Dex-*g*-DOX micelle possesses a therapeutically appropriate diameter and excellent stability. Nanomaterials in this size range generally display favorable pharmacokinetic properties, including the potential for selective accumulation in tumors via the enhanced permeability and retention (EPR) effect.[11] Moreover, the stability of micelle under neutral conditions can reduce the leakage of the drug in the blood circulation.

The *in vitro* release behaviors of DOX from Dex-*g*-DOX were monitored in PBS at pH 4.0, 5.0, 6.8, and 7.4 (Figure 2). The results showed that no significant initial burst release was observed from Dex-*g*-DOX, and less than 49.1% of bound DOX was released within 72 h at pH 7.4. The stability of Dex-*g*-DOX allows for prolonged blood circulation time with minimal release of DOX in the initial phase of administration. In contrast, as the pH was reduced to 6.8, 5.0, and 4.0, the cumulative DOX release of Dex-*g*-DOX was increased up to 60.4%, 72.1%, and 82.5%, respectively. The faster release at pH 5.0 and 4.0 results from the rapid hydrolysis of the acid-sensitive amide linkage in Dex-*g*-DOX under acidic conditions. The stimuli-responsive design of Dex-*g*-DOX enhances the delivery of payload to the lesion site, thereby enhancing the overall therapeutic efficacy and reducing side effects *in vivo*.

To further verify the feasibility of Dex-*g*-DOX for intracellular chemotherapeutic drug delivery, the cell uptake and intracellular release behavior of Dex-*g*-DOX were evaluated by confocal laser scanning microscopy (CLSM) and flow cytometry (FCM). As shown in Figure S4A, B, Supporting Information, HepG2 cells were cocultured with either Dex-*g*-DOX or DOX·HCl, and the signal intensity of DOX·HCl in the cells was significantly higher than that of Dex-*g*-DOX at 2 h. The phenomenon should be attributed to the slowly sustained DOX release from Dex-*g*-DOX in the cells. Next, the inhibition of cell proliferation was evaluated for Dex-*g*-DOX and DOX· HCl against HepG2 cells, as measured *in vitro* by methyl thiazolyl tetrazolium (MTT) test. As shown in Figure S5, Supporting Information, Dex-*g*-DOX exhibited lower antiproliferation efficacy than DOX·HCl after coincubation for 48 h. The result should be due to their different routes of uptake; DOX·HCl could easily diffuse across the cell membrane, while Dex-*g*-DOX was internalized through the endocytic pathway, and the latter might confer relatively more inefficient cell uptake and weaker cytotoxic efficiency.[8] Finally, the antiproliferative activities of Dex-*g*-DOX and DOX·HCl were quantitatively assessed in order to calculate the half-maximal inhibitory concentration (IC_{50}). According to these calculations, Dex-*g*-DOX exhibited a higher IC_{50} (i.e., 2.3 μg mL^{-1}) compared to DOX·HCl (i.e., 0.8 μg mL^{-1}). By these parameters, Dex-*g*-DOX demonstrated less antitumor efficacy relative to DOX·HCl *in vitro* because of its slowly intracellular drug release. It is noteworthy that polymer–drug conjugates have obvious advantages in the complex conditions *in vivo* in comparison to free drug, such as selective intratumoral accumulation through the EPR effect and intracellular drug release triggered by the microenvironments.[2]

Next, the hepatic targeting effect of each DOX formulation was determined *in vivo*. BALB/c mice received a single intravenous injection of either Dex-*g*-DOX or DOX·HCl at an equivalent dose of DOX·HCl at 5.0 mg per kg of body weight (mg (kg BW)$^{-1}$) and were observed postinjection. As shown in Figure 3A, the liver had stronger DOX fluorescence intensity than other organs (i.e., heart, spleen, lung, and kidney). The fluorescence signal of DOX·HCl in the liver became progressively weaker over time. More interestingly, the Dex-*g*-DOX signal exhibited a strong increase from 1 to 24 h. To further evaluate the hepatic targeting ability of the two formulations, the fluorescence intensities were analyzed semi-quantitatively (Figure 3B). At 1 h postinjection, the fluorescence intensity of DOX·HCl in the liver was 2.0-fold higher than that of Dex-*g*-DOX. Amazingly, at 12 and 24 h, the intensity of Dex-*g*-DOX in the liver was 2.7 and 10.2 times higher than that of DOX·HCl, respectively. The enhanced signal of Dex-*g*-DOX compared with DOX·HCl is likely due to the characteristics of highly selective intrahepatic accumulation and sustained DOX release. The ultraselective accumulation of Dex-*g*-DOX in liver should be attributed to the high affinity of polysaccharides for the liver because liver cells such as hepatocytes and Kupffer cells exhibit lectin-like receptors, which demonstrate significant recognition of saccharide residues.[12] The sustained drug release would be assigned to the high stability in physiological conditions and intracellular acidity-sensitivity of Dex-*g*-DOX. In addition to whole-organ studies, liver slices were examined by CLSM, and semi-quantitative analysis of DOX fluorescence intensity showed that DOX kinetics were analogous at the cellular level (Figure S6, Supporting Information). In addition, almost no DOX signal was observed in other major internal organs, such as the heart, spleen, lung, and kidney. Cumulatively, these results demonstrate the highly efficient hepatic targeting ability of the Dex-containing conjugate.

To further explore the clinical efficacy of Dex-*g*-DOX, an *in vivo* model of orthotopic hepatoma was established by administering Sprague–Dawley (SD) rats with *N*-nitrosodiethylamine (DEN) given in their drinking water for more than 10 weeks. Once tumors formed, the hepatoma-bearing animals were treated with Dex-*g*-DOX, DOX·HCl, or normal saline (NS) as a control specifically. Treatment was given every 3 days by intravenous injection at an equivalent DOX·HCl level of 2.0 mg (kg BW)$^{-1}$. Every 2 weeks, three rats from each group were sacrificed under isoflurane anesthesia, and liver tissues were isolated and washed with NS. Next, the tumor nodules (TNs) on the surface of each liver lobe were counted and measured by size. As shown in Figures 4 and 5, fewer TNs were visible in rats treated with either Dex-*g*-DOX or DOX·HCl compared to control. However, Dex-*g*-DOX had significantly stronger antitumor activity than DOX·HCl. Specifically, at the time points of 3 and 5 weeks, the number of large TNs (>3 mm) was 1.9- and 2.1-fold higher in rats treated with DOX·HCl compared to Dex-*g*-DOX ($P < 0.01$; Figure 4A). For the TNs from 1 to 3 mm in diameter (Figure 4B), Dex-*g*-DOX also revealed significantly fewer TNs and higher antitumor efficacy. Finally, in order to further validate the antitumor activity of Dex-*g*-DOX, a terminal deoxynucleotidyl transferase (TdT)-mediated dNTP nick end labeling (TUNEL) assay was performed to study *in situ* tumor cell apoptosis. As shown in Figure 5, the fluorescence intensity was highest in hepatoma treated with Dex-*g*-DOX, indicating significant formation of late-apoptosis DNA. The tumor inhibition property of

Dex-*g*-DOX likely results from its ultraselective accumulation at the tumor site and efficient DOX release within tumor cells.

In clinical practice, various DOX formulations have serious side effects of cardiotoxicity and nephrotoxicity. Therefore, *in vivo* evaluation of off-target effects is another significant step in clinical assessment of antitumor drugs. In our study, the safety of Dex-*g*-DOX was evaluated through histopathological analyses of the major internal organs (i.e., heart, spleen, lung, and kidney). As shown in Figure S7, Supporting Information, DOX·HCl displayed features of myocardial damage and shrunken glomeruli. However, after modifying DOX with Dex, these side effects were significantly decreased or eliminated. All in all, Dex-*g*-DOX exhibited many characteristics of an effective antitumor agent.

In summary, an acid-sensitive polymer–drug conjugate, i.e., Dex-*g*-DOX, is facilely and precisely synthesized. The polymer prodrug forms into micelle after a direct dissolution approach with resulting diameter of around 100 nm, which is a suitable scale for enhanced accumulation in the tumor site via the EPR effect. Dex-*g*-DOX is also favorably biodistributed owing to the self-targeting effect of Dex. Additionally, Dex-*g*-DOX exhibits acid-responsive release of DOX, further enhancing drug delivery to the intracellular microenvironment. Finally, Dex-*g*-DOX promotes significant therapeutic efficacy in the DEN-induced orthotopic hepatoma in rats, surpassing the parent drug both in efficacy and in elimination of toxic side effects. Overall, this study demonstrates that the polysaccharide-modified drugs with tumor microenvironment-sensitive linkers have great potential in the field of clinical hepatoma chemotherapy.

Acknowledgments

All authors give our sincere thanks to Elizabeth M. Higbee-Dempsey from the School of Medicine at the University of Pennsylvania for reviewing and editing the manuscript. This research was financially supported by National Natural Science Foundation of China (Grant Nos. 51303174, 51390484, 51321062, and 51473165). This work was also supported in part by the National Institutes of Health NCI R01CA175480 (ZC).

ABBREVIATIONS

CLSM	confocal laser scanning microscopy
CMC	critical micelle concentration
DBC	drug binding content
DBE	drug binding efficiency
DBR	drug binding rate
DEN	*N*-nitro-sodiethylamine
Dex	dextran
D_h	hydrodynamic diameter
DLS	dynamic light scattering

DOX	doxorubicin
EPR	enhanced permeability and retention
FCM	flow cytometry
FT-IR	Fourier-transform infrared
^{1}H NMR	proton nuclear magnetic resonance
IC_{50}	half-maximal inhibitory concentration
mg (kg BW)$^{-1}$	mg per kg of body weight
MTT	methyl thiazolyl tetrazolium
NS	normal saline
PBS	phosphate-buffered saline
SD	Sprague–Dawley
TEM	transmission electron microscopy
TN	tumor nodule
TUNEL	terminal deoxynucleotidyl transferase (TdT)-mediated dNTP nick end labeling
UV–vis	ultraviolet–visible

References

1. Kopecek J. Polymer-Drug Conjugates: Origins, Progress to Date and Future Directions. Adv Drug Delivery Rev. 2013; 65(1):49–59.
2. Larson N, Ghandehari H. Polymeric Conjugates for Drug Delivery. Chem Mater. 2012; 24(5):840–853. [PubMed: 22707853]
3. Xu W, Ding J, Li L, Xiao C, Zhuang X, Chen X. Acid-Labile Boronate-Bridged Dextran-Bortezomib Conjugate with Up-Regulated Hypoxic Tumor Suppression. Chem Commun. 2015; 51(31):6812–6815.
4. Basu A, Kunduru KR, Abtew E, Domb AJ. Polysaccharide-Based Conjugates for Biomedical Applications. Bioconjugate Chem. 2015; 26(8):1396–1412.
5. Xu H, Ma H, Yang P, Zhang X, Wu X, Yin W, Wang H, Xu D. Targeted Polymer-Drug Conjugates: Current Progress and Future Perspective. Colloids Surf, B. 2015; 136:729–734.
6. Lazarovits J, Chen YY, Sykes EA, Chan WCW. Nanoparticle-Blood Interactions: the Implications on Solid Tumour Targeting. Chem Commun. 2015; 51(14):2756–2767.
7. Gaowa A, Horibe T, Kohno M, Tabata Y, Harada H, Hiraoka M, Kawakami K. Enhancement of Anti-Tumor Activity of Hybrid Peptide in Conjugation with Carboxymethyl Dextran *via* Disulfide Linkers. Eur J Pharm Biopharm. 2015; 92:228–236. [PubMed: 25801495]
8. Xu W, Ding J, Xiao C, Li L, Zhuang X, Chen X. Versatile Preparation of Intracellular-Acidity-Sensitive Oxime-Linked Polysaccharide-Doxorubicin Conjugate for Malignancy Therapeutic. Biomaterials. 2015; 54:72–86. [PubMed: 25907041]
9. Runge A, Hu J, Wieland M, Bergeest J-P, Mogler C, Neumann A, Géraud C, Arnold B, Rohr K, Komljenovic D, Schirmacher P, Goerdt S, Augustin HG. An Inducible Hepatocellular Carcinoma

Model for Preclinical Evaluation of Antiangiogenic Therapy in Adult Mice. Cancer Res. 2014; 74(15):4157–4169. [PubMed: 24906623]

10. Wang K, Kievit FM, Sham JG, Jeon M, Stephen ZR, Bakthavatsalam A, Park JO, Zhang M. Iron-Oxide-Based Nanovector for Tumor Targeted siRNA Delivery in an Orthotopic Hepatocellular Carcinoma Xenograft Mouse Model. Small. 2016; 12(4):477–487. [PubMed: 26641029]
11. Kobayashi H, Watanabe R, Choyke PL. Improving Conventional Enhanced Permeability and Retention (EPR) Effects; What is the Appropriate Target. Theranostics. 2014; 4(1):81–89.
12. Yamaoka T, Tabata Y, Ikada Y. Body Distribution Profile of Polysaccharides after Intravenous Administration. Drug Delivery. 1993; 1(1):75–82.

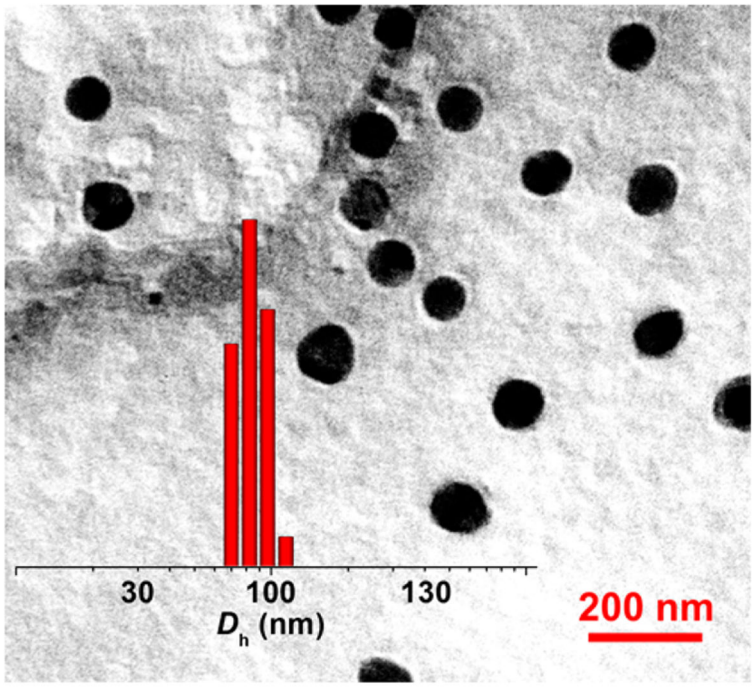

Figure 1.
Representative TEM image and D_h (insert) of Dex-*g*-DOX micelle in PBS. Scale bar: 200 nm.

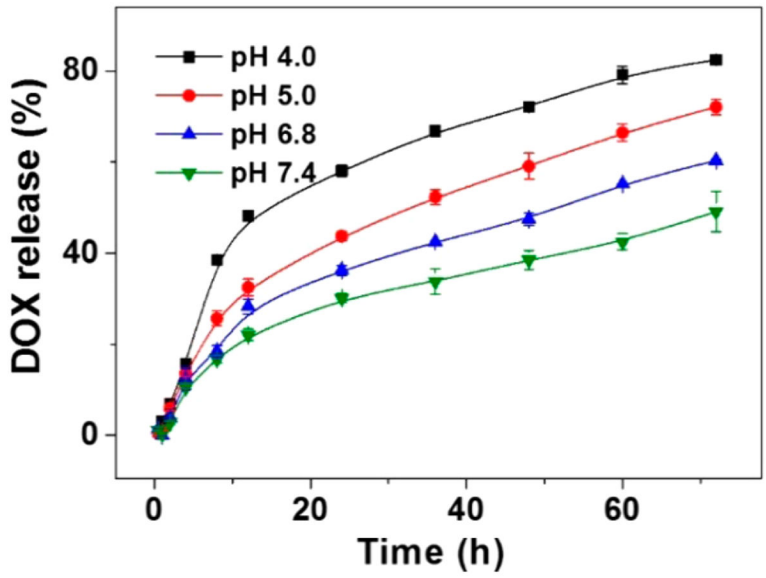

Figure 2.

Release profiles of Dex-*g*-DOX in PBS of pH 4.0, 5.0, 6.8, and 7.4 at 37 °C. Data are presented as a mean ± standard deviation ($n = 3$).

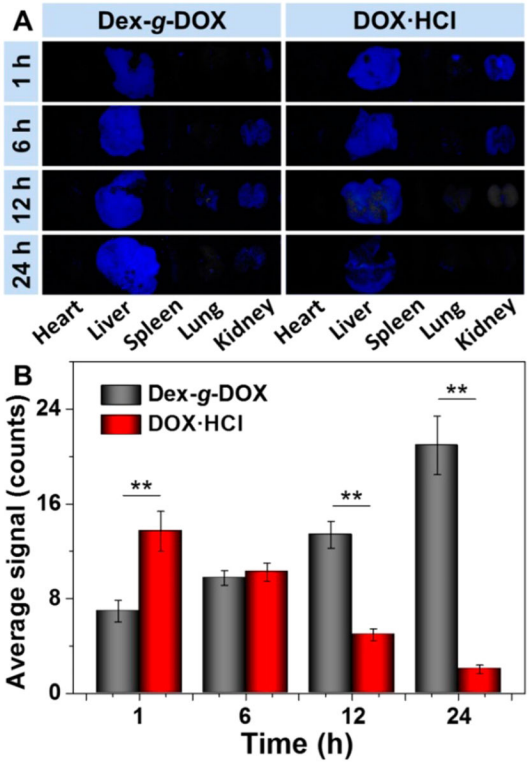

Figure 3.

Biodistribution of Dex-*g*-DOX and DOX·HCl examined in BALB/c mice at 1, 6, 12, or 24 h postinjection. (A) *Ex vivo* DOX fluorescence images of major visceral organs (i.e., heart, liver, spleen, lung, and kidney). (B) Semiquantitatively analyzed average fluorescence intensities of livers. Statistical data are presented as a mean ± standard deviation ($n = 3$; $^{**}P < 0.01$).

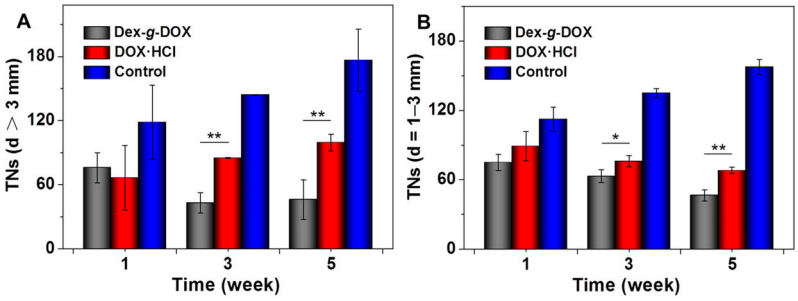

Figure 4.

Antihepatoma efficacies of Dex-*g*-DOX, DOX·HCl, and NS as a control toward a rat hepatocellular carcinoma model. TNs was counted on the liver of each rat: (A) TNs with diameters > 3 mm; (B) TNs with diameters = 1–3 mm. Data are presented as a mean ± standard deviation ($n = 3$; *$P < 0.05$, **$P < 0.01$).

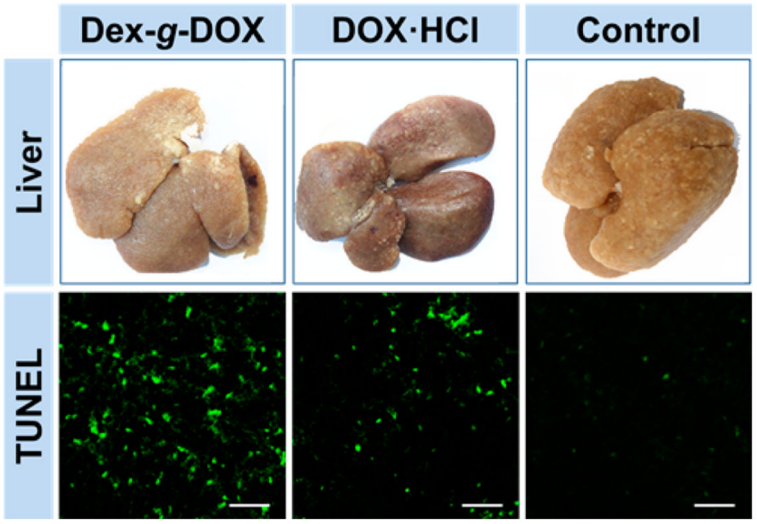

Figure 5.

Apparent photos of the livers and *ex vivo* apoptosis analyses (TUNEL) of liver sections from hepatoma rats at 5 weeks after treatment with Dex-*g*-DOX, DOX·HCl, or NS as a control. Scale bars: 50 μm.

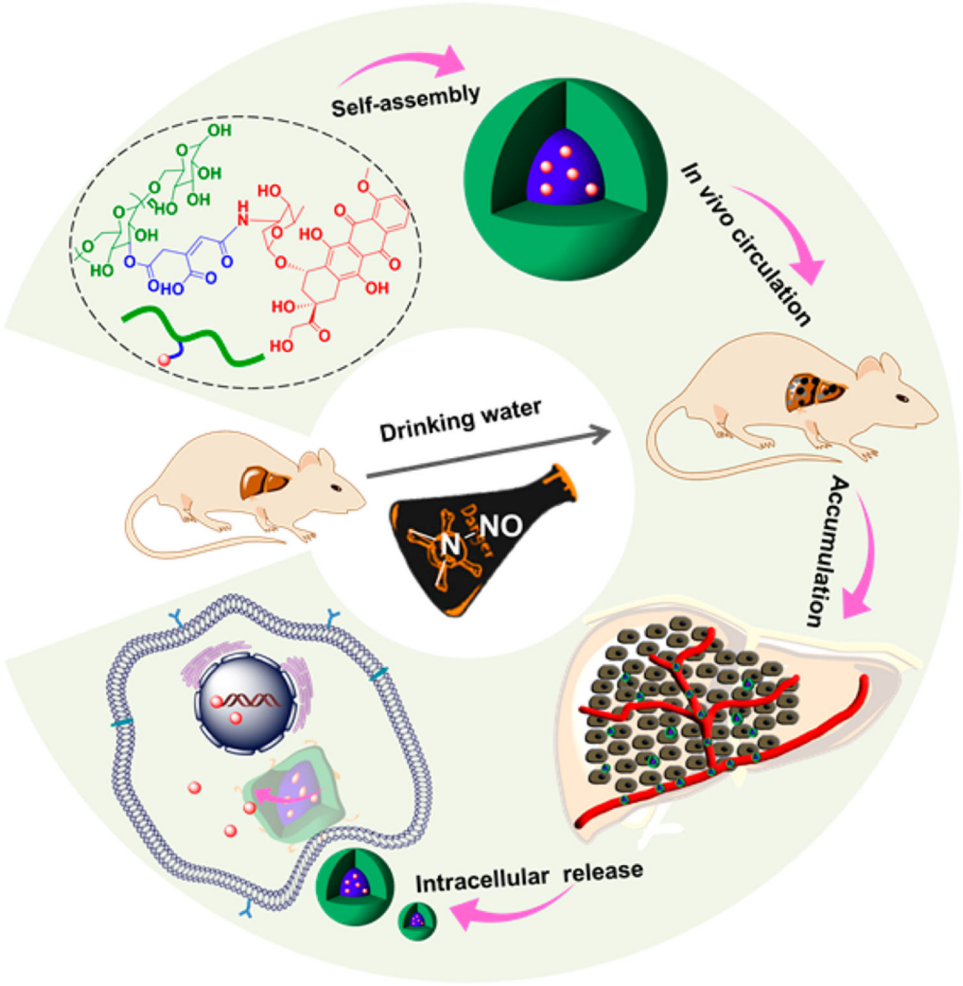

Scheme 1.

Schematic Illustration for Self-Assembly, *in Vivo* Circulation, Selective Accumulation in Tumor Tissue, and pH-Triggered Intracellular DOX Release of Dex-*g*-DOX